Dynamic wetting with viscous Newtonian and non-Newtonian fluids

2009 J. Phys.: Condens. Matter 21 464126

(http://iopscience.iop.org/0953-8984/21/46/464126)

J. Phys.: Condens. Matter **21** (2009) 464126 (12pp) doi:10.1088/0953-8984/21/46/464126

Dynamic wetting with viscous Newtonian and non-Newtonian fluids

Y Wei[1,2], E Rame[3], L M Walker[2,4] and S Garoff[1,2,5]

[1] Department of Physics, Carnegie Mellon University, USA
[2] Center for Complex Fluids Engineering, Carnegie Mellon University, USA
[3] National Center for Space Exploration Research, USA
[4] Chemical Engineering Department, Carnegie Mellon University, USA

Received 4 May 2009
Published 29 October 2009
Online at stacks.iop.org/JPhysCM/21/464126

Abstract
We examine various aspects of dynamic wetting with viscous Newtonian and non-Newtonian fluids. Rather than concentrating on the mechanisms that relieve the classic contact line stress singularity, we focus on the behavior in the wedge flow near the contact line which has the dominant influence on wetting with these fluids. Our experiments show that a Newtonian polymer melt composed of highly flexible molecules exhibits dynamic wetting behavior described very well by hydrodynamic models that capture the critical properties of the Newtonian wedge flow near the contact line. We find that shear thinning has a strong impact on dynamic wetting, by reducing the drag of the solid on the fluid near the contact line, while the elasticity of a Boger fluid has a weaker impact on dynamic wetting. Finally, we find that other polymeric fluids, nominally Newtonian in rheometric measurements, exhibit deviations from Newtonian dynamic wetting behavior.

Introduction

Dynamic wetting is ubiquitous in nature and technology, yet many questions about the origins of the variation of dynamic wetting with contact line speed remain open. Some of these questions arise from the unknown nature of the hydrodynamics in a microscopic region at the contact line. However, the dynamic wetting of viscous fluids is not highly sensitive to those hydrodynamics. Rather, dynamic wetting of viscous fluids depends mostly on the fluid flow slightly farther from the contact line where the physics governing the flow is known and is dominated by the fact that the flow is confined to a wedge-like region whose shape is largely independent of the macroscopic geometry. This region forms an effective boundary condition for the free surface in the macroscopic regions where, for the speeds that can be attained in wetting, viscous forces are negligible and the interface is essentially static-like. Added richness of dynamic wetting of viscous fluids, such as polymer melts and solutions, arises because deformation rates imposed on the fluid may induce non-Newtonian behavior within the wedge-like region controlling the wetting.

Our goal in this paper is to explore how and to what extent such non-Newtonian behavior near the contact line impacts dynamic wetting. We will mainly focus on fluid advancing across a non-deformable solid surface with an inviscid vapor phase above. First, we will review some of the general characteristics of the flow field in the wedge-like region. After describing the particular experimental method we use to probe dynamic wetting, we will show an analytic model for dynamic wetting that very successfully describes dynamic wetting of a specific suite of Newtonian fluids. We then examine the dynamic wetting of two fluids chosen because they exhibit two different types of non-Newtonian behavior in a well controlled fashion. Finally, we see that the dynamic wetting of polymer melts and solutions which appear Newtonian in rheometric measurements—perhaps even most polymer melts and solutions—show deviations from Newtonian behavior.

1. Nature of flow near a moving contact line

Mass conservation requires that in the geometry of the wedge-like region near a moving contact line, the deformation rates in the fluid rise as U/r, where r is the distance from the contact line and U is the speed of the contact line relative to the solid surface. (See figure 1.) For a Newtonian fluid, the stresses also rise as $\eta U/r$, where η is the viscosity of the liquid. Dussan and Davis provide a very general description of how this flow causes a multi-valued

[5] Author to whom any correspondence should be addressed.

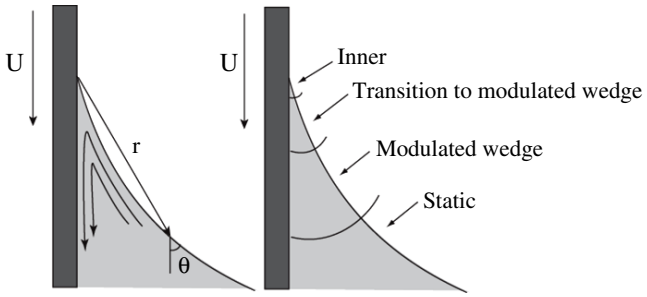

Figure 1. Schematic of wedge-like flow field with coordinate system (left) and regions (right).

velocity field at the contact line and how a resulting non-integrable stress singularity arises in a Newtonian fluid that does not slip on the solid surface, unless some new mechanism intervenes [1]. Many mechanisms that could remove this unphysical stress singularity have been suggested by analysis and simulation, including slip at the solid/liquid interface (see for example [2, 3]), thin films moving ahead of the contact line (see for example [4]), disjoining pressure [5], spatially varying surface tensions [6, 7], or the molecular kinetics model [8], but none have been directly observed experimentally. If a fluid shear thins to zero viscosity, the singularity would be alleviated [9]. While non-Newtonian behavior arising from memory in the fluid cannot alone relieve the multi-valued velocity field, there is no general proof that some constitutive relation containing fluid memory cannot alleviate the stress singularity [3]. As we shall see, the qualitative nature of the wedge flow just outside the 'inner' region where the stress singularity is relieved is not dependent on the detailed nature of these 'inner' physics. We have noted schematically the presence of the inner region in figure 1.

Outside of this inner region, but still in a region where viscous forces on the free surface compete with capillary forces to determine the interface shape, the fluid flow is dominated by the geometrical confinement of the fluid into a wedge-like region. Flow in the wedge has one dominant shear deformation rate proportional to U/r with a dependence on azimuthal position in the fluid. Other deformation rates, both shear and elongation, are smaller by a factor Ca ($=\eta U/\sigma$, capillary number, where σ is the surface tension at the free surface). The elongational deformation rates may become dominant near a stagnation point such as occurs at the entrance to a pre-existing film or at the contact line if slip is the physics operating in the inner region. Due to the rising dominant deformation rate in the flow field, the free surface shows viscous bending which, like the deformation rates, grows as $1/r$.

To make our picture of this wedge-like region more concrete, we refer to a specific description of the flow. We will emphasize the generality of this description. Details of this model may be found in [10] and [11]. For a Newtonian fluid to O(Ca) and with $Re = 0$ ($=\rho U\ell/\sigma$, Reynolds number, where ℓ is a characteristic length scale and ρ is the fluid density), the steady state interface shape in the wedge-like region is given by:

$$\theta = g^{-1}\left(d_0 + Ca\left\{\ln\frac{r}{a} + d_1\right\}\right), \qquad (1)$$

where $g(x) \equiv \int_0^x (y - \sin y \cos y)/2\sin y\,\mathrm{d}y$, a is the length scale associated with the macroscopic scale of the problem, and d_0 and d_1 are constants of integration that can be related to parameters of the inner and outer regions by asymptotic matching. This solution represents the order Ca correction to a static interface arising from viscous bending in the modulated wedge near the contact line. For small arguments $g(x) \sim x^{1/3}$ and if $d_0 = 0$, the variation of free surface slope is $\theta \sim Ca^{1/3}$, a general property of wedge flow which is also found in lubrication analyses (see for example [12]).

To complete the problem, this solution is asymptotically matched to regions on either side of the modulated wedge: to an outer region, with length scale a, where the viscous bending of the interface has become negligible and the interface shape is static-like, and to a region at smaller r which has a length scale ℓ_1. The only requirement on this region at smaller r is that it asymptotically behave as $Ca\ln r$ as $r/\ell_1 \to \infty$ and that $\ell_1 \ll a$. (See figure 1.) This region need not be the region where the stress singularity is alleviated. The composite solution for the interface shape valid in the wedge and its overlap with the outer macroscopic region is [11]:

$$\theta = g^{-1}\left(g(\omega_0) + Ca\ln\frac{r}{a}\right) + f\left(\frac{r}{a}; \omega_0, \frac{a}{R_T}\right) - \omega_0. \qquad (2)$$

On the right-hand side of this equation, the f-function term represents a static-like outer shape, existing far from the contact line where viscous forces are negligible and described by the Laplace equation. ω_0 is the extrapolation of the static shape, f, back to the solid surface. It is not necessarily an angle on the interface but is a precisely defined quantity which can be determined independent of the magnification of any optical system used to measure it.

The interface shape described in equation (2) can only describe the interface in a region where the details of the smaller scale physics have died away and only its asymptotic form, $Ca\ln r$, is significant. This delay of the modulated wedge region (described by equation (1)) until the physics on a smaller scale has relaxed to have the proper $Ca\ln r$ form has been seen for a meniscus advancing over a pre-existing fluid film. Analyses identify parameter ranges where a significant region of r exists in which the flow moving onto the pre-existing thin film causes significant viscous bending not described by the modulated wedge solution, but at larger r (before viscous bending becomes insignificant) the modulated wedge behavior is recovered [13, 14]. We have observed this behavior experimentally as reported in [14] and in section 3 of this paper.

The theory relates the variation of the dynamic contact angle, ω_0, with Ca to parameters describing the physics on the smaller length scale; and it forces the functional form of the viscous bending described by the modulated wedge solution to control the variation of ω_0

$$g(\omega_0) = g(\theta_s + A(U)) + Ca\ln(a/\ell_1(U)), \qquad (3)$$

where θ_s is the static contact angle when $U = 0$ and $A(U)$ is some unknown function of the physics on the smaller scale. The solution also allows the length scale of the smaller scale

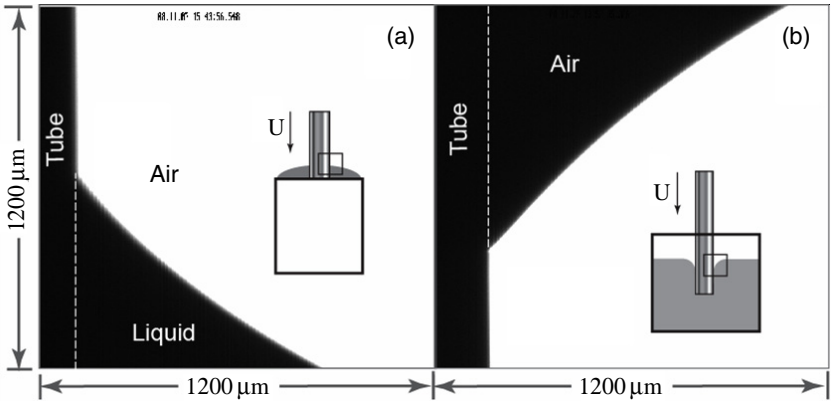

Figure 2. Typical shadows of images. (a) Low Ca with $\omega_0 < 90°$; (b) high Ca with $\omega_0 > 90°$.

physics, $\ell_1(U)$, to vary with contact line speed. If we assume that $A(U)$ and the speed dependence of ℓ_1 have negligible impact and that we remain at small enough arguments of the $g(\omega_0)$ that only the first term in its expansion are needed, then

$$\frac{\omega_0^3}{9} - \frac{\theta_s^3}{9} = Ca \ln \frac{a}{\ell_1}. \tag{4}$$

Here we see explicitly that the modulated wedge flow gives rise to this specific dependence of the dynamic contact angle on Ca. When $\theta_s = 0$, equation (4) also arises naturally in lubrication analyses of moving contact lines which are restricted by definition to small interface slopes.

The $1/r$ dependence of the shear deformation rates as we move to smaller r through the wedge flow region and toward the true inner region suggests that there could be regions where relaxation modes caused by segmental and chain motions of polymeric and even oligomeric fluids will be unable to relax, leading to non-Newtonian behavior in the fluid. Such a region of non-Newtonian behavior will be present if the rising deformation rates anywhere in the flow field cross the inverse of the longest relaxation time in the fluid. Since non-Newtonian behavior need not alleviate the stress singularity, such a non-Newtonian region could intervene between the inner region that resolves the singularity and the region where the modulated wedge flow described by equation (1) dominates. We have indicated the possible presence of such a region in figure 1.

2. Experimental tools

Our goal is to experimentally probe the hydrodynamics that control dynamic wetting. Thus, we want to make measurements at the smallest possible scale with accuracy and precision that allows us to measure the free surface shapes and flow fields predicted by models under well defined contact line motions. Further, we want to expose the wedge flows as much as possible, so we chose geometries that minimize the effect of outer flows (e.g., stagnation points in the center of slots), allowing the wedge flow to manifest itself over larger distances from the contact line.

To achieve these goals, we measure the shape of a meniscus rising on the outside of a vertical cylinder moving into a fluid bath at controlled speeds. Details of all of methods for measuring free surface shapes may be found in [14–18] while the additional methods needed to measure the flow fields are given in [19, 20]. We form a shadow of the meniscus and image it using telemicroscopy and digital image analysis. Typical images of these menisci are shown in figure 2 for examples of menisci with $\omega_0 < 90°$ for smaller Ca (where the meniscus forms above the bulk fluid level) and menisci at larger Ca where the large viscous deformations in the wedge flow region have driven $\omega_0 > 90°$ (and the meniscus forms below the bulk fluid level). Koehler illumination allows us to examine interfaces as close to the contact line as possible, usually within 15–20 μm for interfaces forming angles greater than about 20° with the solid surface and smaller distances as that angle decreases. By viewing from the side, we are able to measure interfaces that approach the solid at angles above or below 90°. The use of a cylinder provides a clear plane of focus for the telemicroscope. We use a larger diameter cylinder ($R_T \approx 10a$ where a is the capillary length of the fluid, $\sqrt{\sigma/(\rho G)}$) and correct all predicted interfaces for the surface being cylindrical rather than flat. We directly extract the interface angle as a function of position along the interface from the gray levels in the image to eliminate the noise we find if we extract the interface position and differentiate to get the interface angle. To ensure the accuracy and precision of the methods, before any dynamic interfaces are measured, the system is calibrated until it can reproduce the known shape of an axisymmetric static meniscus rising on the outside of a cylinder [21].

Our experimental geometry enhances our ability to cleanly probe the wedge-like flows and our control of immersion speeds allows us to probe both steady state and transient motion of the contact line under constant outer length scale conditions. Since our fluid baths have dimensions on the order of $\sim 100a$, the length scale of all flows arising in the outer regions has been moved as far away from the wedge region as possible under terrestrial condition. By immersing the cylinder at fixed speeds, we control contact line speeds and impose any speed we choose in the contact line, unlike in spontaneous spreading of drops. We can also make step changes in the cylinder velocity and examine the transients in the contact line velocity as it moves to a new steady state.

Table 1. 'Newtonian' PDMS melt properties.

Fluids	θ_s@Pyrex (deg, $\pm 5°$)	η@25 °C (P, $\pm 5\%$)	σ (dyn cm^{-1})	M_w [52] (g mol^{-1})	Degree of polymerization
1P	0	1	19.9 ± 0.4	5 970	81
10P	0	10	20.6 ± 0.5	28 000	378
50P	0	47	20.6 ± 0.8	49 350	667
300P	0	282	20.7 ± 0.9	91 700	1239

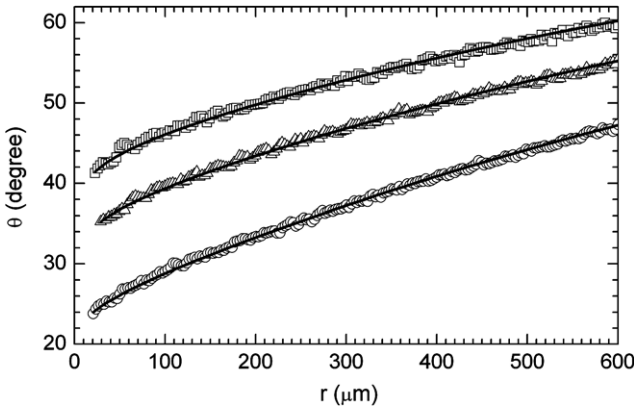

Figure 3. Typical PDMS interfaces for $Ca < 0.01$. (○) $Ca = 0.001$, (△) $Ca = 0.003$, (□) $Ca = 0.005$. Solid line fits to equation (2).

3. A viscous Newtonian fluid

We first examine the dynamic wetting of lower molecular weight polydimethylsiloxane (PDMS) melts which are considered Newtonian fluids. Table 1 describes the properties of the fluids tested. Their steady state interface shapes and flow fields are very well described by the model in equation (2) for $Ca \leqslant 0.1$ [16, 19, 22]. As shown in figure 3, we see that the viscous bending of the interface is very well described by the modulated wedge flow down to the smallest r resolved by our optics ($\sim$20 μm).

In figure 4(a), we show that the dynamic contact angle for these materials follows the approximate relationship in equation (4) for a fluid with zero static contact angle and for low enough Ca that the approximation $g(\omega_0) \approx \omega_0^3/9$ is valid. By changing the chemistry of the solid surface, we change the static contact angle and still observe this same behavior [23]. From these results, we see the connection between the modulated wedge flow dominating over large regions of the interface near the contact line and the $Ca^{1/3}$ power law behavior of the dynamic contact angle. A more detailed analysis of the ω_0 versus Ca data from these fluids allows us to extract some information about the physics at the smaller scales. We find that the velocity-dependent functions $A(U)$ and $\ell_1(U)$ must make small contributions to the variation of ω_0. These variations are material-specific and the U-dependence does not scale with Ca [24]. The ω_0 variation also does not follow models proposed for a short precursing film continuously moving ahead of the contact line [17, 25]. Figure 4(b) shows the variation of the dynamic contact angle to the highest Ca possible in dynamic wetting when air is entrained onto the solid surface. Angles in this

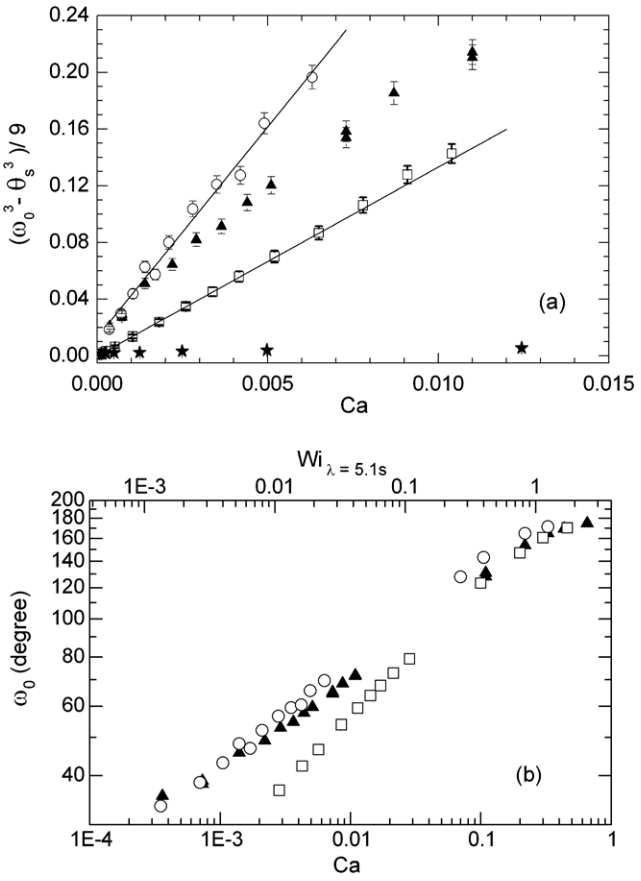

Figure 4. (a) Variations of ω_0^3 versus Ca for (□) 10P PDMS, (★) 0.15 wt% XG solution, (▲) PIB Boger fluid, and (○) PIB base fluid at low Ca. (b) Variation of ω_0 versus Ca over entire Ca range for (□) 600P PDMS, (○) PIB base fluid, and (▲) PIB Boger fluid. Note that the non-zero static contact angle causes the lower slope of the data for the PIB fluids compared to the PDMS.

regime are too large to use the approximation $g(\omega_0) \approx \omega_0^3/9$, so one must use the full $g(\omega_0)$ given below equation (1) to describe these data. The turn over in the data at high Ca is largely due to the form of the g-function, with possibly small contributions from the functions $A(U)$ and $\ell_1(U)$.

Responses to transients forced on the speed of the solid surface exhibit quasi-steady behavior described by this steady state model. After a brief entrance time on the order of 1 s, the interface shapes are described by equation (2) with Ca set to its instantaneous value. At this point, the flow has entered a quasi-steady regime. In figure 5, we show the relaxation of a meniscus after a rapid step change ($\sim$1/30 s) in surface speed. The timescale of the full relaxation to steady state at the new Ca is governed by the viscous relaxation timescale, $\eta a/\sigma$ [26].

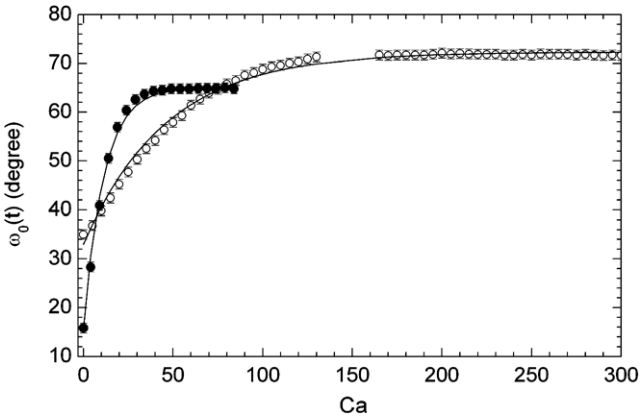

Figure 5. Relaxation of ω_0 for (●) PDMS Ca step up from 0.000 24 to 0.014 and (○) PIB Boger fluid Ca step up from 0.000 36 to 0.011. Solid lines are the fits using viscous time constant [26].

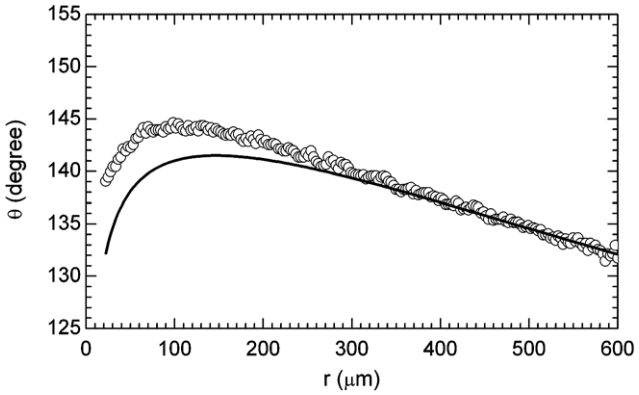

Figure 6. Interface shape of PDMS at $Ca = 0.33$ with $\omega_0 > 90°$. Solid line fit to equation (2).

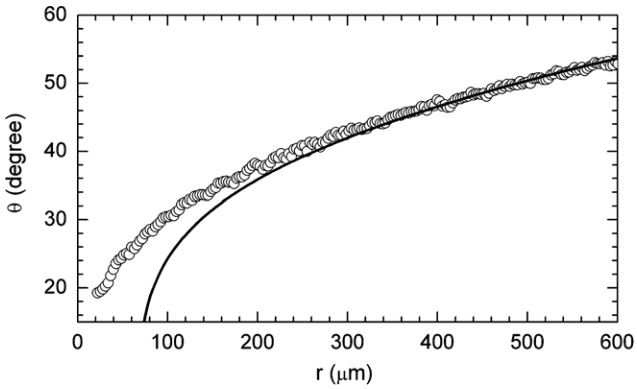

Figure 7. Interface shape of PDMS advancing at $Ca = 0.014$ over pre-existing 10 μm thick film. Solid line fit to equation (2).

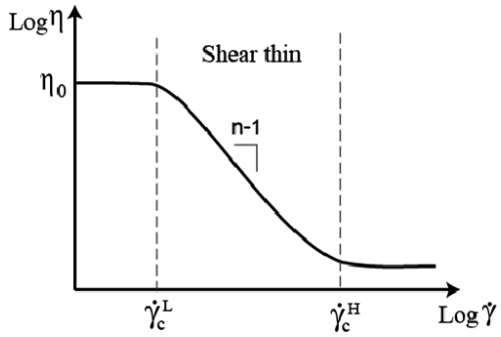

Figure 8. Schematic of rheology for a shear thinning fluid. Solid line represents the shear-rate-dependent viscosity.

In two cases, we have observed extended regions where the viscous bending is no longer well described by the modulated wedge flow in equation (1). The first occurs when we raise the Ca in the fluid beyond $Ca = 0.1$ [27]. (See figure 6.) Here $\omega_0 = 160°$ and the interface has been driven below the bulk level. The region where modulated wedge flow describes the interface shape has been driven out to >500 μm from the contact line. For this case, we cannot be sure whether this delayed onset of the modulated wedge flow arises from an intrinsic inadequacy of the low-Ca theory of equation (1) or from an inability of the physics at some smaller scale to relax such that it can match to the modulated wedge flow described by equation (1). A clearer example is seen in figure 7 where we have shown the interface of a fluid advancing over a pre-existing thin film. For $r > 400$ μm, the interface shows viscous bending is well described by the modulated wedge flow; but for $r < 400$ μm, it is not. Analysis [13] and numerical simulations [14] show this arises because the flow existing in the thin film takes some distance to relax before it can match to the modulated wedge flow. The size of this region depends on both Ca and the thickness of the pre-existing film [14]. As the region described by the modulated wedge becomes larger, the relation of ω_0 to Ca becomes better described by the 1/3 power law arising from the wedge flow [14].

These results for lower molecular weight PDMS show that the viscous bending in the melts of these highly flexible polymers is well described by equation (1). In fact, the full model in equation (2) describes all aspects of the dynamic wetting of these fluids very well for $Ca < 0.1$. Dynamic contact angles behave as expected when the modulated wedge flow describes most of the region of the interface showing viscous bending. We do see cases where some physics on a smaller length scale delays the onset of the wedge flow until larger r. To probe the impact of non-Newtonian behavior on dynamic wetting, we now examine the wetting of two types of fluids carefully designed to exhibit well controlled non-Newtonian behavior.

4. Non-Newtonian fluids: shear thinning

Since fluid elements experience high-shear rates near a moving contact line, we expect significant effects on dynamic wetting when the viscosity of the fluid is shear-rate dependent. In this section, we focus on the impact of shear thinning. Figure 8 illustrates how the viscosity varies with shear rate for an idealized shear thinning fluid. The viscosity shows a zero-shear plateau at η_0 for shear rates less than a lower critical shear rate, $\dot{\gamma}_c^L$, and then decreases following a power law with exponent, $n-1$. For anything but a superfluid, the viscosity again plateaus

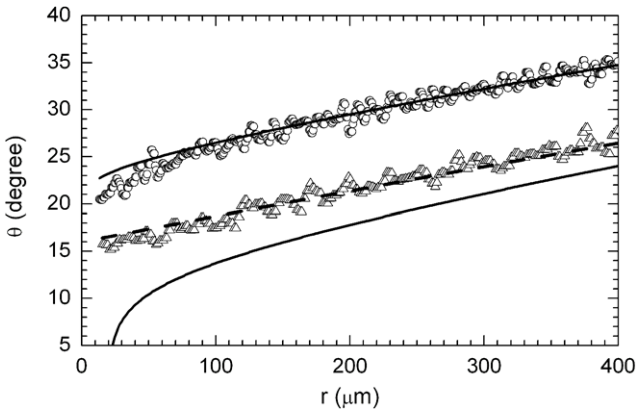

Figure 9. Interface shapes of (△) 0.15 wt% XG solution at $Ca = 0.0005$ and (○) 2% PEO solution at $Ca = 0.0006$. Dashed line fit to static interface shape for XG data. Solid line best fits to equation (2) for both XG and PEO data. For the XG case, the fit to equation (2) cannot match the data at all because of the large curvature required by Ca.

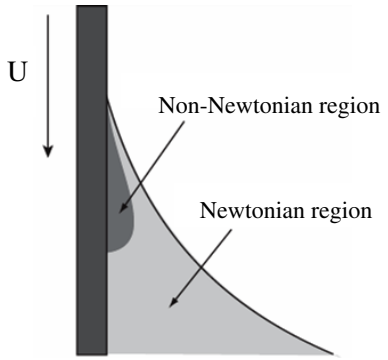

Figure 10. Newtonian and non-Newtonian regions for a shear thinning fluid.

for shear rates above an upper critical shear rate, $\dot{\gamma}_c^H$. The shear thinning exponent n is material dependent and varies between 0 and 1, with $n = 1$ for a Newtonian fluid.

We use dilute aqueous solutions of a semi-flexible polymer, xanthan gum (XG), to probe the impact of shear thinning [28, 29]. The XG solution we will discuss here has $n = 0.4$ and $\dot{\gamma}_c^L = 0.1\ s^{-1}$. No measurable fluid memory effects (first normal stress difference are not seen above the low limit of the instrument $N_1 < 0.5$ Pa) are observed for shear rates between 10^{-3} and $10^2\ s^{-1}$. Figure 9 shows a typical interface of the XG solution. We see that viscous bending is virtually absent and the interface is described by a static shape. No part of the interface is described by the modulated wedge flow using a Ca based on the zero-shear viscosity, η_0, of the solution or any other viscosity other than zero. A mechanism (described by a model below) has dramatically reduced the interface curvature, which implies that the viscous component of the normal stress on the free surface, $\Delta\tau$, (=total normal stress $- \rho g z$, where z is the vertical distance from a given point on the interface to the bulk fluid level) is largely removed. Figure 4(a) shows the variation of ω_0 with Ca is greatly reduced from the behavior that is observed for fluids where modulated wedge flow dominates the viscous bending of the interface.

Lubrication analysis may be used to obtain the flow field and the interface shape for this type of shear thinning fluid [28]. As shown in figure 10, a region near the free surface exists where the shear rates remain below $\dot{\gamma}_c^L$ and the fluid exhibits Newtonian behavior. In a region extending along the solid until the shear rate drops below $\dot{\gamma}_c^L$, the fluid exhibits shear thinning behavior. For the $\dot{\gamma}_c^L$ of the XG solution shown in figure 9, we estimate this region extends to a distance $\sim$ 1mm, beyond the field of view of the experiment. This analysis successfully mimics the trends seen in our experiments. From the model, we see that the reduction in the viscous bending arises from the reduction of the fluid viscosity along the solid wall in the region extending from the contact line, reducing the drag of the solid on the fluid. This reduction on the wedge flow reduces both viscous bending and the variation of the dynamic contact angle with Ca. Studies of drop spreading of shear thinning fluids suggest similar behavior [30, 31].

Dilute polyethylene oxide (PEO) aqueous solutions also shear thin. The 2 wt% PEO solutions we have examined have a low critical shear rate, $\dot{\gamma}_c^L = 10\ s^{-1}$, and a shear thinning exponent of $n \sim 0.8$ [32]. However, they also show a large first normal stress difference, which is a manifestation of fluid memory. Figure 9 compares the interfaces of the XG and PEO solutions at similar Ca. Unlike XG, an extended region of viscous bending described by modulated wedge flow is recovered in PEO. Also, in the region where the viscous bending is not described by modulated wedge flow, the interface curvature of the PEO solution is enhanced (rather than reduced, as in the XG solution) compared to a Newtonian fluid with the same zero-shear viscosity. Thus, while the impact of shear thinning in PEO likely reduces the drag of the solid on the fluid in a region along the solid to distance on the order of 100 μm, we observe very different dynamic wetting behavior than in XG. Motivated by the presence of fluid memory in the PEO solution, we attempt to isolate the impact of fluid memory using the well controlled fluid discussed in section 5.

5. Non-Newtonian fluids: elasticity

Fluid elasticity, or fluid memory, causes a time-dependent relaxation of the responding viscous stress in the fluid after adding or removing a load. Most elastic fluids have complex relaxation spectra. In this section, we discuss a simple case, an elastic fluid with only one relaxation mode that can be described by the Oldroyd-B constitutive equation [33]. Two parameters are used to characterize its rheology, viscosity and relaxation time. Figure 11 illustrates how this fluid responds under sinusoidal shear deformations over a wide range of frequencies, ω. The dynamic viscosity η' ($\equiv G''/\omega$, where G'' is the viscous modulus) is a measure of energy dissipation. It is constant for an Oldroyd-B fluid, just as for a Newtonian fluid. However, unlike a Newtonian fluid, the elastic fluid shows a non-zero first normal stress coefficient $\Psi_1(\omega)$ ($\equiv 2G'/\omega^2$ in the linear viscoelastic limit, where G' is the elastic modulus) which is a measure of energy storage. For an Oldroyd-B elastic

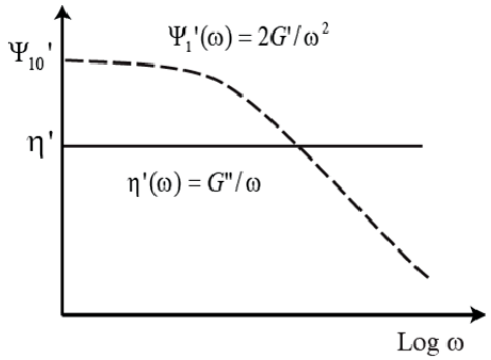

Figure 11. Schematic of rheology for a Oldroyd-B fluid. Solid line represents the shear-rate-independent viscosity. Dashed line represents the first normal stress difference coefficient.

fluid, the value of $\Psi_1(\omega)$ increases as the frequency decreases and finally forms a plateau in the low frequency (small-shear rate) region with a value of Ψ_{10}. In the Oldroyd-B model, the relaxation time of this fluid is $\lambda = \Psi_{10}/2\eta_0$, where η_0 is the zero-shear rate viscosity of the fluid. We use a Weissenberg number ($Wi = \lambda U/a$) based on the capillary length to characterize the potential strength of the impact of elasticity on the dynamic wetting in the geometry of our experiments.

Boger fluids are well-established model elastic fluids that were designed to exhibit rheology described by the Oldroyd-B constitutive equation [33, 34]. With a high, constant viscosity provided by an oligomeric, Newtonian base fluid and a slow relaxation mode provided by a small amount of high molecular weight polymer additive, Boger fluids can be used to isolate elastic effects from significant shear thinning and inertial effects [35]. Since a Boger fluid is a solution, we replace the zero-shear rate viscosity in the calculation of relaxation time with $\Delta\eta = \eta_0 - \eta_s$, which is the viscosity contribution from the component of the fluid that is adding elasticity to the solution.

We have examined the dynamic wetting behavior of several Boger fluids based on polyisobutylene (PIB) and polystyrene (PS) [29, 36, 37]. As an example of the dynamic wetting behavior we have observed in these fluids, we discuss a PIB Boger fluid with $\lambda = 5$ s relaxation time. This fluid was prepared by dissolving 0.3 wt% high molecular with PIB (4.7×10^6 g mol^{-1} PIB, Scientific Polymer Products, Inc.) into its oligomer melt (Indopol® H-100, Innovene Inc.) with less than 5 wt% kerosene to assist the dissolution. Its wetting behavior up to a Ca approaching air entrainment (where ω_0 approaches 180°), was examined. To isolate the impact of the elasticity of the Oldroyd-B mode of the fluid, we compare its dynamic wetting to that of its Newtonian base.

Figure 12(a) shows interface shapes of our Boger fluid at increasing Ca and Wi; figure 12(b) shows the distance from the contact line, r_c, where for $r > r_c$ the interface shape is described by equation (2). For interfaces with $\omega_0 < 90°$ (menisci forming above the bulk fluid level), the region where viscous bending is described by equation (2) is delayed to increasing distances from the contact line as Ca increases. For smaller distances from the contact line, $r < r_c$, the interface

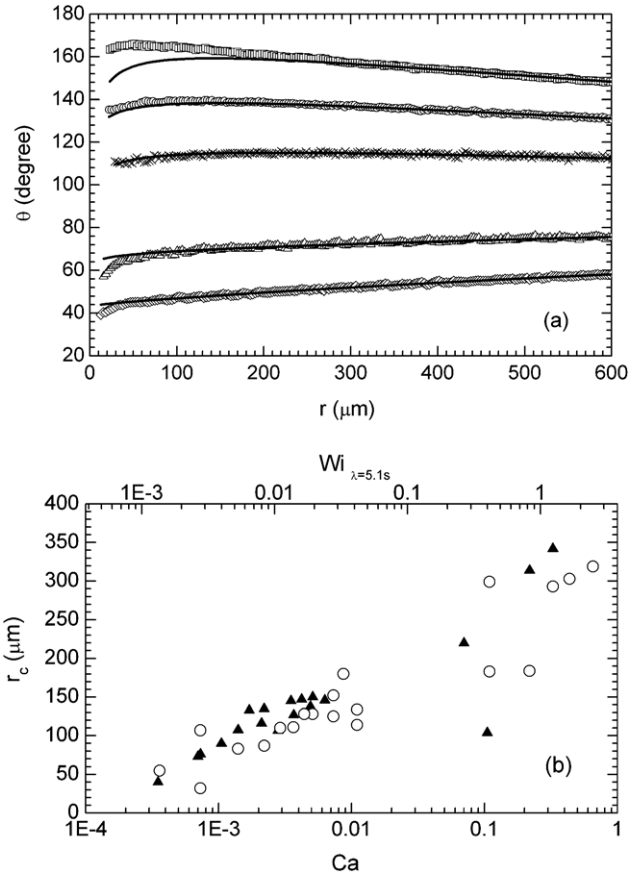

Figure 12. (a) Variation of the interface shapes with Ca for PIB Boger fluid. (◇) $Ca = 0.0014$, (△) $Ca = 0.011$, (×) $Ca = 0.11$, (○) $Ca = 0.22$, (□) $Ca = 0.65$. Solid line fits to equation (2). (b) Variation of r_c versus Ca for (○) PIB Boger fluid and (▲) PIB base fluid.

is more curved[6] than predicted by equation (2). For these low Ca's, Wi is quite small; yet, we see a detectable difference in the wetting of the Boger fluid from the predicted behavior for a Newtonian fluid. Since the perturbations from the Newtonian interface shapes are small, we use the Newtonian flow fields [10] to determine the largest distance near the solid wall where the shear rate in the fluid is greater than the inverse Oldroyd-B relaxation time of the fluid, thus characterizing the region where non-Newtonian behavior might be occurring. For all the cases with $\omega_0 < 90°$, this distance is comparable to the region where the modulated wedge fails to describe the viscous bending, i.e., $r < r_c$. To determine if this behavior is due to the elasticity added by the Oldroyd-B mode, we must compare the dynamic wetting of the Boger fluid to that of its Newtonian oligomer base. In figures 12(b) and 13, we see that at these low Ca's, the base and Boger fluids have virtually identical behavior. Thus, the differences in the dynamic wetting of the Boger fluid from a Newtonian fluid are not arising from the long Oldroyd-B relaxation mode added by the high molecular weight specie. They are already present in the Newtonian base fluid—a subject we will discuss further in section 6.

[6] The interface curvature is estimated from the slope of the r–θ plot with ∼5% accuracy.

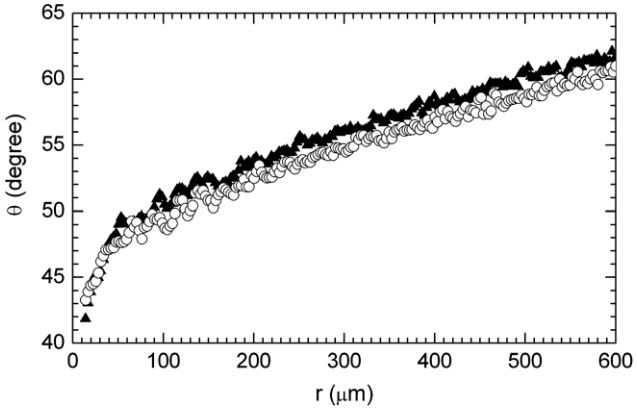

Figure 13. Comparison of the interface shapes for (○) PIB Boger fluid and PIB base (▲) fluid at $Ca = 0.0022$.

The behavior at higher Ca and Wi where $\omega_0 > 90°$ leads to a similar conclusion but is more complex to observe from the data. When the meniscus is below the bulk fluid level, the static part of the normal stress at the interface causes a negative curvature, while the viscous bending for the advancing menisci contributes a positive curvature. Thus in figure 12(a), we see an inflection point in the interface (zero slope in our r–θ plots) which moves to small r as Ca increases. As shown in figure 12(b), the region where the viscous bending is described by modulated wedge flow continues to retreat to larger r. This behavior is also present in the Newtonian base fluid. In figure 14(a), we compare the Boger and base fluids at the same $Ca = 0.33$ for a case where $\omega_0 > 90°$. For this case Wi of the Boger fluid is 1.2, while Wi for the base fluid (using some very fast relaxation time in the fluid) is orders of magnitude smaller. Again, estimating from the theory for Newtonian flow fields, the deformation rates near the solid wall are large enough to prevent relaxation of the segmental and chain motions of high molecular weight polymer additive to $r = 100$ μm in the Boger fluid, well within the region directly observed in the experiment. Figure 14(b) shows the viscous component of the normal stress at the free surface is larger in the PIB Boger fluid than in its oligomer base fluid. However, much of this increase comes from the fact that the viscosity of the Boger fluid is 1.9 times that of the oligomer base. Therefore, the velocity gradients at the interface of the PIB Boger fluid are quite similar to those of its oligomer base fluid. The difference we see in figure 14(b) mainly comes from the viscous contribution of the high molecular weight additive rather than its elastic contribution, further evidence that the elasticity of the Oldroyd-B relaxation mode has little impact on the interfaces. It is apparent from these results that the elastic non-Newtonian behavior of the long relaxation modes in the Boger fluid in the high-shear region near the solid surface is not effective in bending the free surface and impacting dynamic wetting.

The variation of the dynamic contact angle ω_0 with Ca for the Boger fluid and the Newtonian base is shown in figure 4(a) for lower Ca. We see the variation of ω_0 with Ca for Boger fluid is slightly reduced compared to its Newtonian base, but both are very close to the $Ca^{1/3}$ behavior arising from the

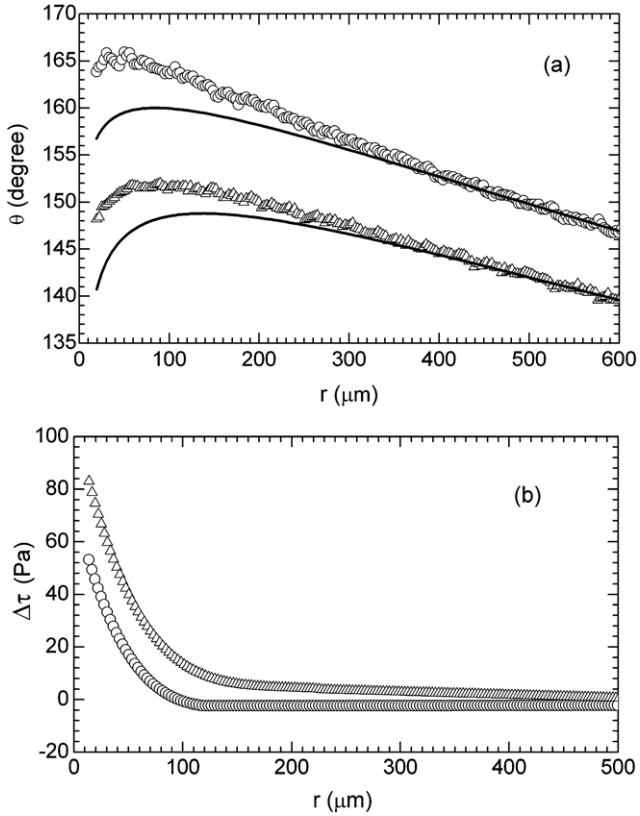

Figure 14. Comparison of (△) PIB Boger fluid and (○) PIB base fluid at $Ca = 0.33$ with $\omega_0 > 90°$. (a) Interface shapes with best fits to equation (2). (b) Viscous component of the normal stress at the free surface.

fact that modulated wedge flow occupies much of the region where viscous bending is occurring. Differences in the slopes of these curves arise due to different material properties such as ℓ_1 and not from deviations from the modulated wedge flow behavior. However, there does appear to be more deviation for the Boger fluid data from the $Ca^{1/3}$ relation than for the Newtonian base fluid. Figure 4(b) shows the similarity of dynamic contact angles of the Boger and Newtonian base fluids over the entire Ca range examined. As in the examination of the interface shapes, we again see the non-Newtonian behavior of the long relaxation modes in the Boger fluid in the high-shear region near the solid surface is not very effective in impacting the dynamic contact angle. What is most striking is the effectiveness of the shear thinning near the solid surface in altering viscous bending and ω_0 compared to relatively minor impact of the elasticity in the Boger fluid near the solid surface on dynamic wetting, even for an elastic fluid with seconds of memory.

We have also compared the dynamic wetting of this Boger fluid and its Newtonian base fluid in other geometries, including drops spreading on horizontal surfaces and withdrawal of a vertical surface from the fluid bath when a thin film is entrained on the solid. While some small differences appear between these elastic and Newtonian fluids, they are not large.

Since non-Newtonian fluids often show an overshoot in their response to step changes in stress, we studied the

Table 2. 'Newtonian' PIB melt properties.

Fluids	θ_s@Pyrex (deg, ±5°)	η@25 °C (P, ±5%)	σ (dyn cm^{-1})	M_n [53] (g mol^{-1})	Degree of polymerization
L-14	5	0.56	23.4 ± 0.9	370	7
H-7	13	2.7	24.2 ± 0.8	440	8
H-35	24	51	30.5 ± 1.0	700	13
H-100[a]	20	110	31.5 ± 1.0	910	16
300P[b]	23	308	31.7 ± 1.0	950	17
H-300[c]	29	833	32.7 ± 0.9	1300	23

[a] PIB melt used as the Boger fluid solvent, with <5 wt% kerosene in it.
[b] 300P is Parapol 950 sample from Exxon Chemical, others are Indopol® samples from Innovene, Inc.
[c] Shows a small but detectable first normal stress difference.

relaxation of dynamic wetting for the Boger fluid after a step change in surface velocity. For PIB Boger fluids, we observe only a monotonic response with no overshoots in either the contact line position or ω_0 with time after the step change in surface speed. The relaxation of the PIB Boger fluid is correctly described by the same quasi-steady behavior as the PDMS discussed in section 3. An example is given in figure 5 where the viscous time constant for the relaxation, $\eta a/\sigma$, describes the contact angle relaxation of the Boger fluid. In this example, Ca changes from 4×10^{-4} to 0.01 and Wi changes from 1.4×10^{-3} to 0.42. Jumps to larger Ca and Wi could not be completely quantified by our methods since the meniscus moved from above the bulk level to below it which requires two different optical cell geometries. However, we have determined that no overshoot in contact line position occurs even for transients with increases in surface speeds as large as factors of 30, final values of Ca approaching 0.65 (close to air entrainment), and Wi reaching 2.4. At this high a value of Wi, some fraction of the flow field is sampling the nonlinear regime of the fluid, based on the constitutive relation developed from rheometric measurements.

Elasticity is thought to change the threshold for a variety of instabilities in wetting flows [38–43]. We do not observe any instabilities on the free surface of our PIB Boger fluids, even in transients as the surface speed is changed very rapidly (within 1/30 s) and we reach the nonlinear regime mentioned above. In our experiments, Re remains small at all speeds examined and does not show the broken contact line phenomena seen in higher Re cases for both Newtonian [44] and non-Newtonian [38] fluids. Unlike the receding case where the threshold for the 'ribbing instability' is lowered by elasticity [39, 40], the advancing case is predicted to be stable [45].

We have used a lubrication analysis to determine the velocity field and interface shape for an Oldroyd-B fluid in a small region near the contact line [46]. Our methods are based on those used in [4, 47, 48]. We use either a pre-existing thin film or slip on the solid surface to relieve the contact line stress singularity. We perform a double expansion in Ca and Wi for all the governing equations and boundary conditions. Because we only keep the lowest order terms in the elastic correction, the effects of elongational deformations and nonlinear elastic effects are lost. We integrate the 3rd order ordinary differential equation for the interface shape that arises in the lubrication analysis so that it matches to a static macroscopic interface shape in a two-dimensional slot geometry. This 3rd order differential equation has a quadratic behavior as the distance along the solid surface from the contact line, $x \to \infty$ (where x is the distance along the solid surface); but the theory indicates that a region where $\theta \sim (Ca \ln(x))^{1/3}$ will appear for small enough Ca $(a/\ell_1)^{3/2}$. This log behavior is similar to the modulated wedge behavior of the Newtonian case in equation (1). As in previous studies [47, 49, 50] and our experiments, our analysis shows the impact of Oldroyd-B elasticity on the dynamic wetting is weak at the low Wi accessible to these methods and the precise results are significantly influenced by the flow in the outer regions of the slot.

6. Other viscous polymer melts

In section 5, we have seen that for $Ca < 0.01$, the oligomeric, Newtonian PIB base fluid shows deviations from the predictions for a Newtonian fluid which do describe PDMS fluids. Oligomeric PS fluids show similar deviations [51].

To investigate this further, we examined the suite of PIB materials listed in table 2. These PIB oligomer melts appear Newtonian in shear rheometry with only the H-300 PIB melt showing a barely detectable first normal stress difference at the highest-shear rates probed. Figure 15 shows three typical examples of the deviations of the interface shapes from equation (2) which describes the lower viscosity PDMS. As shown in figure 16, the onset of the modulated wedge region always increases with Ca for a given material. However, the behavior across members of the suite of fluids is not simple. For example, in figure 17 we see a fluid that is more viscous, H-300, deviates less from the Newtonian result than a less viscous fluid, H-35. Full characterization of trends in the dynamic wetting across this suite of fluids would require more carefully controlled fluid properties, especially molecular weight polydispersity.

We have eliminated two possible causes for the differences between the PDMS suite of fluids and the other Newtonian fluids. The first is the fact that the PDMS fluids form a zero degree static contact angle with the Pyrex solid surfaces, but the PIB and PS fluids do not. However, when PDMS fluids spread across a fluorinated surface where they have a static

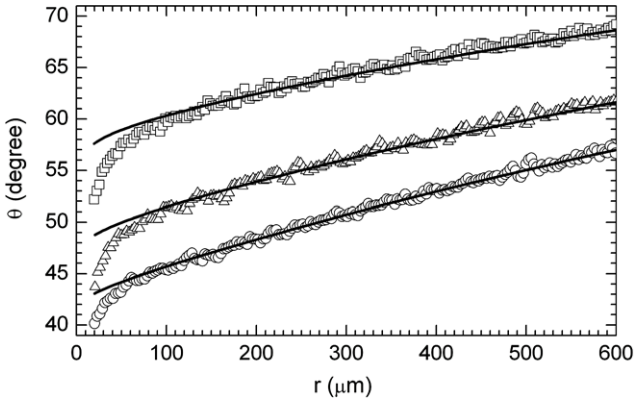

Figure 15. Typical interface shapes of H-35 oligomeric PIB at low Ca. (○) $Ca = 0.0013$, (△) $Ca = 0.0026$, (□) $Ca = 0.0051$. Solid line fits to equation (2).

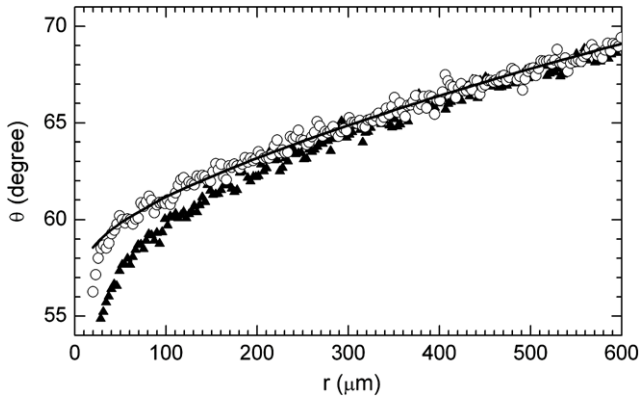

Figure 17. Comparison of interface shapes for (○) H-300 and (▲) H-35 at $Ca = 0.0051$. Solid line fit to equation (2). The best fits to each data set are indistinguishable.

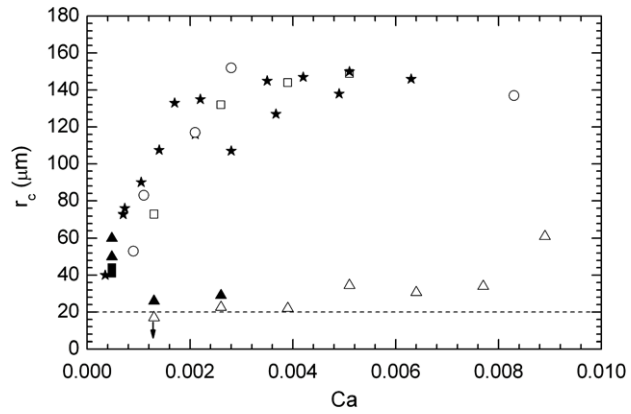

Figure 16. Variation of r_c with Ca for all PIB melts listed in table 2. (■) L-14, (▲) H-7, (□) H-35, (★) H-100, (○) 300P, (△) H-300. Dashed line shows the detectable limit of 20 μm and the error bars of all data are ± 5 μm. Arrow on data for H-300 at $Ca = 0.0013$ indicates it is below the delectability limit.

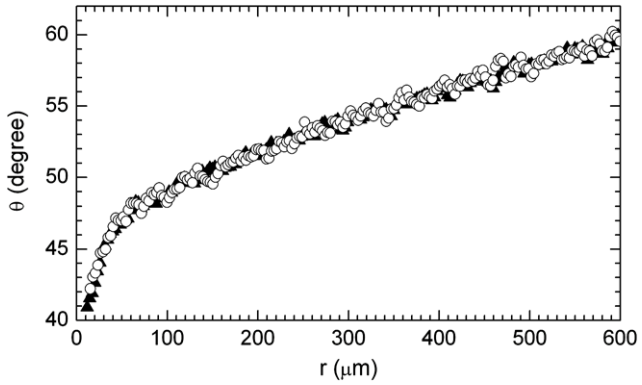

Figure 18. Comparison of the interfaces for H-7 oligomeric PIB at $Ca = 0.0014$ on (▲) a bare Pyrex glass surface and on (○) a methylated surface.

contact angle of ∼50°, we see no delay of the modulated wedge region as we do in the PIB and PS fluids [23]. We also do not see a monotonic change in the deviation for the PIB fluids as the static contact angle increases. These results suggest the deviations in the PS and PIB fluids do not arise from differences in the static contact angle.

We have also shown the delay of the modulated wedge region is not due to the interaction with the solid surface. Figure 18 is the comparison of the interfaces at the same Ca for the same PIB fluid but on different energy surfaces, bare Pyrex and a methylated surface. Clearly the interface shapes are identical. A similar result is found for a Newtonian PS oligomer [51]. Further, there is no significant difference in the variation of onset position of the modulated wedge region, r_c, over the entire range of Ca for the PIB fluid on Pyrex and on the methylated surface. The origin of the delay of the modulated wedge region is a fluid property and not due to interactions with the solid surface.

One intriguing possibility for the origin of the delay of the modulated wedge region is that complex non-Newtonian behavior of these oligomeric fluids is occurring on a small length scale. As discussed earlier, such non-Newtonian behavior is unlikely to alleviate the contact line singularity in the inner region. However, the inverse deformation rates in the flow field cannot rise above the very fast relaxation times in these fluids except very close to the contact line. Therefore, the region where the non-Newtonian behavior is occurring must be on length scales below a micron. Thus, the fluid is Newtonian throughout the field of view of the experiments, in particular in the regions where the viscous bending is not described by the modulated wedge solution. The delay of the modulated wedge region is occurring as the influence of the non-Newtonian behavior at the much smaller length scale relaxes in regions where the fluid is Newtonian. As we have seen, such a transition region also occurs in the case of PDMS advancing over a pre-existing film.

7. Summary

We have investigated the dynamic wetting of viscous Newtonian and non-Newtonian fluids. We have restricted the discussion to viscous fluids to minimize the impact of the inner scale physics (which relieves the contact line stress singularity) on the variation of the dynamic contact angle with Ca. This has allowed us to focus on the wedge flow that dominates

the wetting in these cases. Many aspects of the dynamic wetting (including steady state interface shapes, velocity fields, advancing over dry and pre-wet surfaces, and transients) of Newtonian PDMS fluids are well characterized by a model that describes the wedge flow by the first order correction in Ca to a static interface shape or by lubrication analyses of advancing menisci over pre-existing films. Both modeling approaches assume Newtonian behavior everywhere in the fluid. To begin the examination of dynamic wetting of non-Newtonian fluids, we focused on fluids with well controlled non-Newtonian behavior. Shear thinning fluids greatly reduce the impact of viscous flow by reducing the drag of the solid surface on the fluid in the wedge-like region driving the dynamic wetting. In contrast, the elasticity due to the added high molecular weight polymer solute in Boger fluids has a much smaller impact on dynamic wetting. As we returned to an examination of oligomeric polymer melts which are nominally Newtonian, we saw aspects of the dynamic wetting which suggest these fluids may be exhibiting non-Newtonian behavior on a smaller length scale, and this behavior may be impacting the flow and dynamic interface shapes on a larger length scale.

Acknowledgments

The authors thank all the students who have contributed to the material discussed in this paper including J Marsh, K Willson, Q Chen, K Stoev, X Chen, Y Suo, D Draganov, and G Sevaratnam. We also thank the NSF and NASA for funding for parts of these studies.

References

[1] Dussan E B V and Davis S H 1974 On the motion of a fluid–fluid interface along a solid surface *J. Fluid Mech.* **65** 71–95
[2] Hocking L M 1977 Moving fluid interface. 2. Removal of force singularity by a slip-flow *J. Fluid Mech.* **79** 209–29
[3] Dussan E B V 1976 The moving contact line: the slip boundary condition *J. Fluid Mech.* **77** 665–84
[4] Spaid M A and Homsy G M 1994 Viscoelastic free-surface flows—spin-coating and dynamic contact lines *J. Non-Newton. Fluid Mech.* **55** 249–81
[5] Kalliadasis S and Chang H C 1994 Apparent dynamic contact-angle of an advancing gas–liquid meniscus *Phys. Fluids* **6** 12–23
[6] Shikhmurzaev Y D 1997 Moving contact lines in liquid/liquid/solid systems *J. Fluid Mech.* **334** 211–49
[7] Shikhmurzaev Y D 1993 The moving contact line on a smooth solid-surface *Int. J. Multiph. Flow* **19** 589–610
[8] De Coninck J and Blake T D 2008 Wetting and molecular dynamics simulations of simple liquids *Annu. Rev. Mater. Res.* **38** 1–22
[9] Rosenblat S and Davis S H 1985 How do liquid drops spread on solids? *Frontiers in Fluid Mechanics. A Collection of Research Papers Written in Commemoration of the 65th Birthday of Stanley Corrsin* (Berlin: Springer) pp 171–83
[10] Cox R G 1986 The dynamics of the spreading of liquids on a solid surface. Part 1. Viscous flow *J. Fluid Mech.* **168** 169–94
[11] Dussan E B V, Ramé E and Garoff S 1991 On identifying the appropriate boundary-conditions at a moving contact line—an experimental investigation *J. Fluid Mech.* **230** 97–116
[12] Hocking L M 2001 Meniscus draw-up and draining *Eur. J. Appl. Math.* **12** 195–208
[13] Jensen O E 2000 An advancing meniscus in a prewetted tube private communication
[14] Chen X, Ramé E and Garoff S 2004 The effects of thin and ultra-thin liquid films on dynamic wetting *Phys. Fluids* **16** 287–97
[15] Marsh J A 1992 Dynamic contact angles and hydodynamics near a moving contact line *PhD Thesis* Carnegie Mellon University, Pittsburgh
[16] Ramé E and Garoff S 1996 Microscopic and macroscopic dynamic interface shapes and the interpretation of dynamic contact angles *J. Colloid Interface Sci.* **177** 234–44
[17] Stoev K *et al* 1998 The effects of thin films on the hydrodynamics near moving contact lines *Phys. Fluids* **10** 1793–803
[18] Stoev K, Ramé E and Garoff S 1999 Effects of inertia on the hydrodynamics near moving contact lines *Phys. Fluids* **11** 3209–16
[19] Chen Q, Ramé E and Garoff S 1997 The velocity field near moving contact lines *J. Fluid Mech.* **337** 49–66
[20] Chen Q 1996 Experimental investigation of dynamic wetting models: interface shapes and velocity fields near the moving contact line *PhD Thesis* Carnegie Mellon University, Pittsburgh
[21] Huh C and Scriven L E 1969 Shapes of axisymmetric fluid interfaces of unbounded extent *J. Colloid Interface Sci.* **30** 323–37
[22] Marsh J A, Garoff S and Dussan E B V 1993 Dynamic contact angles and hydrodynamics near a moving contact line *Phys. Rev. Lett.* **70** 2778–81
[23] Willson K R 1995 The dynamic wetting of polymer melts: an investigation of the role of material properties and the inner scale hydrodynamics *PhD Thesis* Carnegie Mellon University, Pittsburgh
[24] Ramé E, Garoff S and Willson K R 2004 Characterizing the microscopic physics near moving contact lines using dynamic contact angle data *Phys. Rev.* E **70** 031608
[25] Eggers J and Stone H A 2004 Characteristic lengths at moving contact lines for a perfectly wetting fluid: the influence of speed on the dynamic contact angle *J. Fluid Mech.* **505** 309–21
[26] Suo Y *et al* 2001 Hydrodynamics and contact angle relaxation during unsteady spreading *Langmuir* **17** 6988–94
[27] Chen Q, Ramé E and Garoff S 1995 The breakdown of asymptotic hydrodynamic models of liquid spreading at increasing capillary number *Phys. Fluids* **7** 2631–9
[28] Seevaratnam G K *et al* 2007 Dynamic wetting of shear thinning fluids *Phys. Fluids* **19** 012103
[29] Seevaratnam G K 2006 Dynamic wetting of non-Newtonian fluids *PhD Thesis* Carnegie Mellon University, Pittsburgh
[30] Carre A and Eustache F 2000 Spreading kinetics of shear-thinning fluids in wetting and dewetting modes *Langmuir* **16** 2936–41
[31] Rafai S and Bonn D 2005 Spreading of non-Newtonian fluids and surfactant solutions on solid surfaces *Physica* A **358** 58–67
[32] Suo Y 2001 Unsteady spreading of Newtonian fluids and dynamic wetting of shear thinning fluids *PhD Thesis* Carnegie Mellon University, Pittsburgh
[33] Binnington R J and Boger D V 1985 Constant viscosity elastic liquids *J. Rheol.* **29** 887–904
[34] Boger D V 1977/78 A highly elastic constant-viscosity fluid *J. Non-Newton. Fluid Mech.* **3** 87–91
[35] Boger D V and Nguyen H 1978 A model viscoelastic fluid *Polym. Eng. Sci.* **18** 1037–43
[36] Wei Y *et al* 2007 Dynamic wetting of Boger fluids *J. Colloid Interface Sci.* **313** 274–80

[37] Wei Y, Garoff S and Walker L M 2009 Impact of fluid memory on wetting approaching the air entrainment limit *J. Colloid Interface Sci.* at press
[38] Cohu O and Benkreira H 1998 Entrainment of air by a solid surface plunging into a non-Newtonian liquid *AIChE J.* **44** 2360–8
[39] Lopez F V *et al* 2002 Non-Newtonian effects on ribbing instability threshold *J. Non-Newton. Fluid Mech.* **103** 123–39
[40] Grillet A M, Lee A G and Shaqfeh E S G 1999 Observations of ribbing instabilities in elastic fluid flows with gravity stabilization *J. Fluid Mech.* **399** 49–83
[41] Zevallos G A, Carvalho M S and Pasquali M 2005 Forward roll coating flows of viscoelastic liquids *J. Non-Newton. Fluid Mech.* **130** 96–109
[42] Coyle D J, Macosko C W and Scriven L E 1990 Reverse roll coating of non-Newtonian liquids *J. Rheol.* **34** 615–36
[43] Spaid M A and Homsy G M 1997 Stability of viscoelastic dynamic contact lines: an experimental study *Phys. Fluids* **9** 823–32
[44] Blake T D and Ruschak K J 1979 Maximum speed of wetting *Nature* **282** 489–91
[45] Graham M D 2003 Interfacial hoop stress and instability of viscoelastic free surface flows *Phys. Fluids* **15** 1702–10
[46] Wei Y 2009 Dynamic wetting of viscous and viscoelastic fluids *PhD Thesis* Carnegie Mellon University, Pittsburgh
[47] Ro J S and Homsy G M 1995 Viscoelastic free surface flows: thin film hydrodynamics of Hele–Shaw and dip coating flows *J. Non-Newton. Fluid Mech.* **57** 203–25
[48] Park C W and Homsy G M 1984 2-phase displacement in Shaw–Hele cells—theory *J. Fluid Mech.* **139** 291–308
[49] Spaid M A and Homsy G M 1996 Stability of Newtonian and viscoelastic dynamic contact lines *Phys. Fluids* **8** 460–78
[50] Lee A G, Shaqfeh E S G and Khomami B 2002 A study of viscoelastic free surface flows by the finite element method: Hele–Shaw and slot coating flows *J. Non-Newton. Fluid Mech.* **108** 327–62
[51] Seevaratnam G K *et al* 2005 Wetting by simple room temperature polymer melts: deviations from Newtonian behavior *J. Colloid Interface Sci.* **284** 265–70
[52] Data from product property literature of Gelest, I
[53] Data from product literature of Innovene, I